European Journal of Human Genetics (2020) 28:1218–1230
https://doi.org/10.1038/s41431-020-0583-2

ARTICLE

A dominant vimentin variant causes a rare syndrome with premature aging

Benjamin Cogné[1,2] · Jamal-Eddine Bouameur[3] · Gaëlle Hayot[4,5,6,7] · Xenia Latypova[1,2] · Sundararaghavan Pattabiraman[8] · Amandine Caillaud[2] · Karim Si-Tayeb[2] · Thomas Besnard[1,2] · Sébastien Küry[1,2] · Caroline Chariau[9] · Anne Gaignerie[9] · Laurent David[9,10] · Philippe Bordure[11] · Daniel Kaganovich[8,12] · Stéphane Bézieau[1,2] · Christelle Golzio[4,5,6,7] · Thomas M. Magin[3] · Bertrand Isidor[1,2]

Received: 10 July 2019 / Revised: 14 January 2020 / Accepted: 17 January 2020 / Published online: 17 February 2020

Abstract

Progeroid syndromes are a group of rare genetic disorders, which mimic natural aging. Unraveling the molecular defects in such conditions could impact our understanding of age-related syndromes such as Alzheimer's or cardiovascular diseases. Here we report a de novo heterozygous missense variant in the intermediate filament vimentin (c.1160 T > C; p.(Leu387Pro)) causing a multisystem disorder associated with frontonasal dysostosis and premature aging in a 39-year-old individual. Human vimentin p.(Leu387Pro) expression in zebrafish perturbed body fat distribution, and craniofacial and peripheral nervous system development. In addition, studies in patient-derived and transfected cells revealed that the variant affects vimentin turnover and its ability to form filaments in the absence of wild-type vimentin. Vimentin p.(Leu387Pro) expression diminished the amount of peripilin and reduced lipid accumulation in differentiating adipocytes, recapitulating key patient's features in vivo and in vitro. Our data highlight the function of vimentin during development and suggest its contribution to natural aging.

Introduction

Rare genetics syndromes with an accelerated aging have been classified as progeroid syndromes. At the severe end of the spectrum, the early-onset Hutchinson–Gilford progeria is due to heterozygous variants in the intermediate filament protein LMNA (MIM: 150330), encoding lamin A/C [1]. Lamins are nuclear fibrous proteins belonging to the type V family of intermediate filament (IF) proteins and perform structural and regulatory functions [1]. IFs, together with microtubules and actin filaments, form the cytoskeletal framework in the cytoplasm and nucleus of most eukaryotic cells. IFs are divided into six groups based on their primary sequence and tissue-specific expression [2]. Vimentin, a type III IF protein, is widely expressed in all mesenchymal cells. It shares the typical tripartite domain organization with all IF proteins with a central, highly conserved α-helical rod domain mediating vimentin homo- and hetero-dimerization essential for the early stages of vimentin polymerization, flanked by globular head and tail domains responsible for elongation and compaction of fully formed filaments [3]. Vimentin plays major roles in cell shape, maintenance of the overall integrity of the cytoplasm, and in stabilizing cytoskeletal interactions and cell substrate adhesion [4].

Two missense variants in the human vimentin gene have been identified so far in two unrelated individuals diagnosed with cataract [5, 6]. The two variants (c.451 G > A

These authors contributed equally: Benjamin Cogné, Jamal-Eddine Bouameur, Gaëlle Hayot

These authors jointly supervised this work: Christelle Golzio, Thomas M. Magin, Bertrand Isidor

Supplementary information The online version of this article (https://doi.org/10.1038/s41431-020-0583-2) contains supplementary material, which is available to authorized users.

✉ Christelle Golzio
christelle.golzio@igbmc.fr

✉ Thomas M. Magin
thomas.magin@uni-leipzig.de

✉ Bertrand Isidor
bertrand.isidor@chu-nantes.fr

Extended author information available on the last page of the article

p.(Glu151Lys) and c.623 A > G p.(Gln208Arg) are located in coil1A subdomain of vimentin rod and the variant p.(Glu151Lys) has been shown to act in a dominant manner by inducing aggregation of the vimentin network. Transgenic mice expressing a vimentin$^{p.(Arg113Cys)}$ mutant also developed a cataract without obvious other symptoms [7]. This organ-specific disease was surprising, considering the wide tissue expression of vimentin. In line with this unexpected phenotype, the targeted deletion of vimentin in mice caused widespread but mild phenotypes in unchallenged animals [2, 8]. Most recently, the analysis of phospho-deficient vimentin knockin mice indicated a role of vimentin in skin aging, neuronal differentiation, and subcutaneous fat loss [9–11].

Here we report a novel vimentin variant (c.1160 T > C; p.(Leu387Pro)) causing a syndromic disorder affecting craniofacial development, peripheral nervous system, and adipose and ectodermal tissues. The pathogenicity of the variant was confirmed by recapitulating the key clinical features in cellulo and in vivo.

Materials and methods

Exome sequencing

Whole-exome sequencing (WES) was performed with Agilent SureSelect Clinical Research Exome following recommended procedures and samples were sequenced on HiSeq4000 by Integragen SA (Evry, France). Paired-end reads of 75 bp were obtained. Quality of Fastq files was checked by FastQC (v0.11.3), adapters were removed by cutadapt (v1.8.1), and a pipeline following GATK's best practices (v3.4) was performed. Briefly, fastq were aligned on human genome hg19 by bwa mem (v0.7.3), Bam files were sorted, and duplicate reads were filtered out using Picard MarkDuplicates (v1.119). Alignment files were then realigned and base quality recalibrated. Variant calling was performed using HapolypeCaller (GATK) in gVCF (genomic variant calling format) mode and gVCF was genotyped together with 30 other WES gVCFs, to perform variant quality score recalibration. Variants were annotated and filtered using ANNOVAR (ANNOtate VARiation) and in-house python scripts.

Database submission

The variant has been submitted to clinvar and is accessible at: https://www.ncbi.nlm.nih.gov/clinvar/variation/692107/.

Additional procedures are described in the Supplementary Information files.

Results

Clinical features of the affected individual

This study was approved by the review boards of the involved institutions and written informed consents have been obtained from the affected individual and his family. The 39-year-old male proband was born from non-consanguineous parents. At birth, he presented with congenital frontonasal dysostosis that required surgery at the age of 5 years. Thoracic scoliosis was noted at the age of 15 months and worsened, despite orthopedic treatment, requiring surgery at the age of 16 years (Fig. 1a). At the age of 16 years, severe amyotrophy, thin skin, and lipodystrophy were noted with pes cavus, alopecia, absent eyebrows, micrognathia, and oligodontia (Fig. 1a). Electromyography showed a motor and sensitive peripheral neuropathy. At the age of 17 years, a nerve biopsy of the leg revealed a severe axonal loss associated with demyelination. Progressive bilateral sensorineural deafness began at 10 years and required bilateral hearing aid at 15 years old. At the age of 31 years, ophtalmological examination showed a chronic normal tension glaucoma with progressive bilateral cupping of the optic nerves and visual field loss. At the age of 33 years, two episodes of cerebral ischemic strokes occurred (frontal and cerebellar infarcts) with right hemiparesis. Cerebral magnetic resonance imaging showed diffuse cortical atrophy with bilateral ventricular dilatation. A left patella fracture occurred at the age of 36 years. Osteodensitometry showed osteopenia (T-score -2,4 SD). Given the similarity of these clinical features with a mild form of Hutchinson progeria and Werner syndrome, *LMNA* and *WRN* were sequenced but no function-affecting variants have been identified. An array comparative genomic hybridization was performed and did not reveal candidate copy number variations.

Genetic analysis

We performed WES of the DNA from the proband at a depth of 80× and analyzed the data following GATK's best practices (v3.4). We kept variants which were: (1) exonic or at splice sites (±10 bp), (2) with a frequency below 0.5% in gnomAD and our internal database of 1000 exomes, and (3) covered by at least 10 reads and with an allele frequency above 0.2. We identified 245 variants matching those criteria, including 62 variants in known disease-causing genes in OMIM (Supplementary Table S1). For the analysis, in a diagnostic setting, we focused on those disease-causing genes as we suspected it could be a phenotypic expansion of a known disorder. From the 62 variants, none was identified on X-chromosome. One gene, *FDXR*, carried two rare

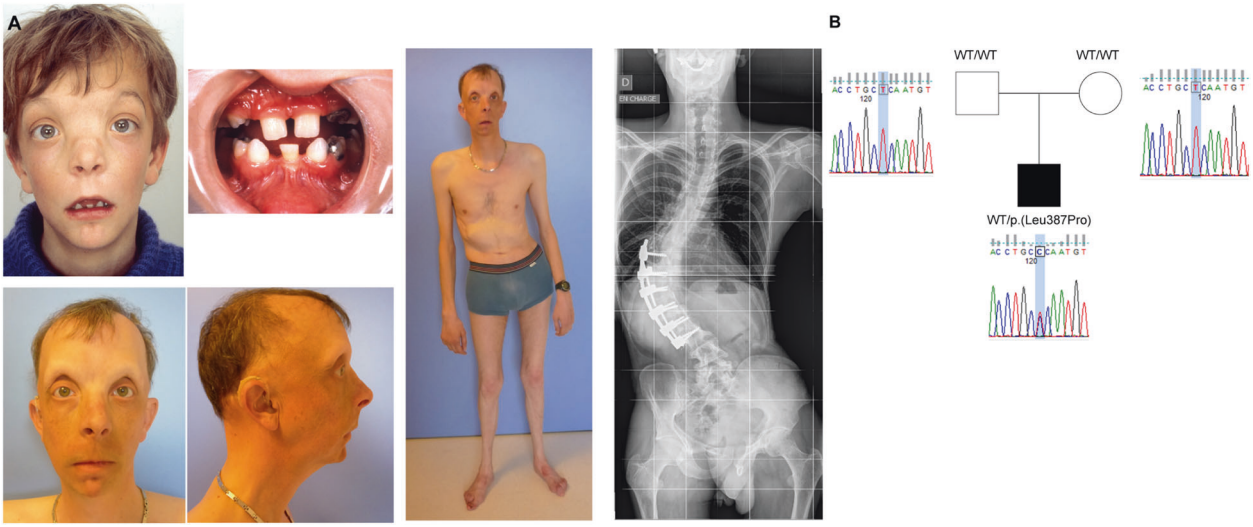

Fig. 1 A vimentin variant is responsible for a syndrome with progeroid features. a Patient in childhood presenting with craniofacial dysostosis and oligodontia and at age 36 years with thin skin, alopecia, absence of facial hairs, micrognathia, fat loss, amyotrophy, and scoliosis. **b** Sanger sequencing electropherogram showing p.(Leu387Pro) in *VIM* in the proband and absent from the parents.

variants and could fit with an autosomal recessive inheritance. *FDXR* is known to cause a syndrome associating an auditory neuropathy and an optic atrophy (MIM: 617717), but the phenotype did not match with the patient's clinical presentation. Then, we analyzed the 19 rare variants associated with an autosomal dominant disorder. No variant has been identified in a gene associated with a syndromic phenotype with aging-related symptoms. Then, given the severity of the phenotype, we kept only variants absent from 1000 genome and gnomAD, and with either a predicted loss-of-function effect or a CADD phred score (v1.3) above 20. We ended up with two missense variants: c.293 C > G p.(Pro98Arg) (GenBank: NM_001130698.1) in *TRPC3* and c.1160 T > C p.(Leu387Pro) (GenBank: NM_003380.4) in *VIM*. *TRPC3* was associated with a spinocerebellar ataxia (MIM: 616410) and *VIM* to cataract (MIM: 116300). We performed segregation analysis for both genes and we found that the variant in *TRPC3* was inherited from the healthy father, and that the *VIM* variant c.1160 T > C p.(Leu387Pro) had occurred de novo (Fig. 1b). We then decided to explore further the *VIM* variant, because vimentin is a type III IF protein, a class of structural proteins related to lamins, a well-known gene causing progeroid syndromes.

The Leucine residue at position 387 in vimentin is highly conserved among the IF superfamily and is located in an "e" position along the α-helical wheel of the coil2 subdomain of the rod (Fig. 2a, c) [3]. Leucine to Proline substitutions at the corresponding position of desmin and KRT17 are associated with myofibrillar myopathy and steatocystoma multiplex, respectively (Fig. 2a) [5, 12]. Structural homology modeling based on the previously crystalized vimentin coil2 subdomain predicted that c.1160 T > C p.(Leu387Pro) variant should not significantly change vimentin static structure (Fig. 2b). Although it should not involve primary misfolding, it could still affect higher-order interactions among vimentin subunits in filaments or with associated proteins.

Characterization of c.1160 T > C p.(Leu387Pro) variant in cultured cells

To examine whether the c.1160 T > C p.(Leu387Pro) variant affected vimentin expression or cytoskeletal organization, induced pluripotent stem (iPS) cells were reprogrammed from mononuclear cells enriched from peripheral blood of the patient and were analyzed by immunofluorescence microscopy. The overall filamentous organization of the vimentin cytoskeleton in patient iPS cells appeared highly similar to that in controls (Fig. 3a and Supplementary Fig. S1A). However, the overall staining intensity and the number of vimentin-positive cells were reduced in the patient's iPS cell population (Fig. 3a and Supplementary Fig. S1A). This prompted us to investigate vimentin protein levels by western blotting and fluorescence-activated cell sorting analysis. This revealed reduced vimentin protein levels (Fig. 3b and Supplementary Fig. S1B). Notably, in the patient's iPS cells, vimentin was processed into distinct fragments of 48 and 25 kDa with little full-length vimentin left (Fig. 3b and Supplementary Fig. S1B). Given that the vimentin antiserum used recognizes a carboxy-terminal vimentin epitope, the fragments detected by western blotting result from cleavage of vimentin at its head domain [13, 14]. This is consistent with a reduced vimentin protein stability caused by the variant. In this setting, the vimentin variant's mRNA levels remained unaffected (Fig. 3c). To examine whether the

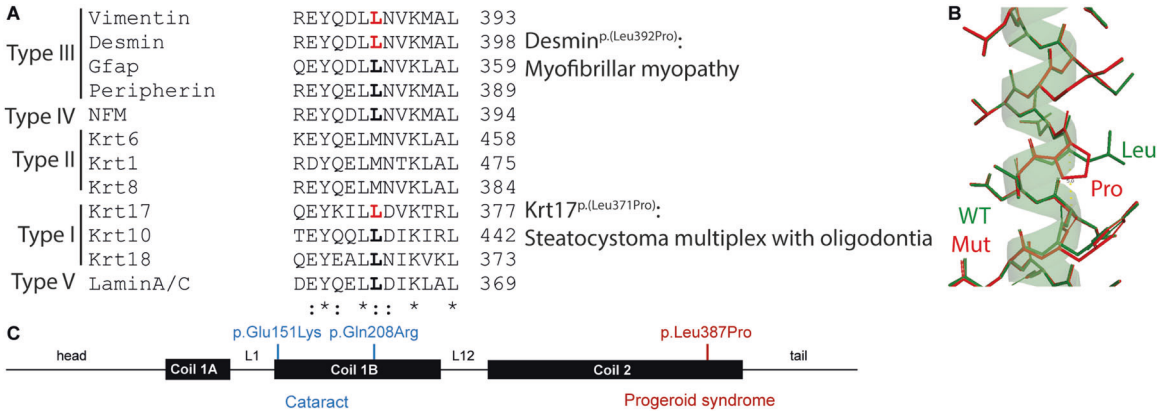

Fig. 2 Vimentin Leucine 387 is highly conserved within the IF family. a Protein sequence alignment of human vimentin with selected other human IF proteins. Vimentin$^{p.(Leu387Pro)}$ patient's variant and the equivalent residues in other IFs are marked in bold. Vimentin$^{p.(Leu387Pro)}$ and known other IFs pathogenic variants at equivalent residues are further marked in red. Note the high degree of conservation of the L residue and the existence of equivalent pathologic L to P variants in desmin and keratin 17, respectively. **b** Protein structure alignment of the previously described wild-type vimentin with a modeled structure of the mutant. **c** Domain organization of vimentin with a central α-helical rod domain (divided into coil 1A, linker 1, coil1B, linker 12, and coil 2) flanked by globular head and tails. The two only reported vimentin missense variants are in the coil 1B and depicted in blue and the newly discovered p.(Leu387Pro) in red. Vimentin$^{p.(Glu151Lys)}$ has been shown to form cytoplasmic aggregate-like structures.

destabilizing effect of the novel vimentin mutant was more general, vimentin wild-type (wt) and the p.(Leu387Pro) mutant were transiently transfected as hemagglutinin (HA)-tagged variants in 3T3-L1 preadipocytes. In analogy to iPS cells, immunofluorescence analysis showed that HA-tagged vimentin$^{p.(Leu387Pro)}$ was co-distributed with the endogenous cytoplasmic vimentin network of 3T3-L1 cells, highly similar to wt vimentin (Fig. 4a). Strikingly, in a minority (<1%) of vimentin$^{p.(Leu387Pro)}$ cells, cytoplasmic aggregate-like structures reminiscent of those seen in other IF disorders were observed [2].

We then investigated the impact of vimentin$^{p.(Leu387Pro)}$ in the absence of endogenous vimentin, following transient expression of wt and/or mutant vimentin in vimentin knockout (KO) mouse embryonic fibroblasts (MEFs) and vimentin-negative MCF-7 cells. In both cell types, vimentin$^{p.(Leu387Pro)}$ was unable to form an extensive filamentous network on its own and accumulated in cytoplasmic aggregate-like structures as depicted by immunofluorescence microscopy (Figs. 4b, c). When co-expressed with wt vimentin, either native or as HA-tagged variant, vimentin$^{p.(Leu387Pro)}$ formed extensive filament networks in the majority of MCF-7 transfectants, although large aggregates were observed in a subset of cells (Fig. 4b). HA-tagged and non-tagged vimentin behaved similarly, showing that the fusion did not affect vimentin behavior.

Thus, vimentin$^{p.(Leu387Pro)}$ forms normal IF in the heterozygous state and negatively influences vimentin protein stability by promoting vimentin proteolysis in a highly selective manner. In analogy to other dominant IF variants, it fails to assemble into filaments in the absence of wt vimentin or other type III/IV IF proteins.

Proteasomal degradation of vimentin$^{p.(Leu387Pro)}$ is accelerated compared with wt vimentin

The decreased abundance of vimentin in the patient's iPS cells (Fig. 3b and Supplementary Fig. S1B) suggested increased vimentin turnover downstream of the c.1160 T > C p.(Leu387Pro) variant (Fig. 3b). We therefore performed immunofluorescence and immunoblotting analyses at several time points post transfection of vimentin-negative MCF-7 cells and vimentin-positive 3T3-L1 cells. Vimentin$^{p.(Leu387Pro)}$ disappeared faster than wt filaments (Figs. 4d, e and Supplementary Fig. S2). Enhanced turnover was confirmed by immunoblotting, revealing that vimentin$^{p.(Leu387Pro)}$ or vimentin$^{p.(Leu387Pro)}$-HA protein levels were systematically lower, leading to a faster clearance of mutant compared with wt vimentin in transfected vimentin KO MEFs, MCF-7 cells, and 3T3-L1 cells (Fig. 4d-f), suggesting that protein stability was affected by the variant. Indeed, treatment of transiently transfected MCF-7 and 3T3-L1 with a proteasome inhibitor caused preferential accumulation of vimentin$^{p.(Leu387Pro)}$ compared with wt vimentin (Figs. 5a, b). To corroborate these findings, we generated 3T3-L1 cells stably expressing either vimentin-HA or vimentin$^{p.(Leu387Pro)}$-HA (3T3-L1/Vim-HA and 3T3-L1/Vim$^{p.(Leu387Pro)}$-HA cells) in addition to endogenous vimentin. In those cells, vimentin$^{p.(Leu387Pro)}$-HA mostly displayed a cytoplasmic filamentous pattern as assessed by immunofluorescence microscopy, confirming that the mutant co-assembled into filaments together with wt vimentin (Supplementary Fig. S3A). The expression levels of vimentin-HA and vimentin$^{p.(Leu387Pro)}$-HA were similar (Supplementary Fig. S3B) but lower than the endogenous one as revealed by a two-dimensional electrophoresis, which enables separation of

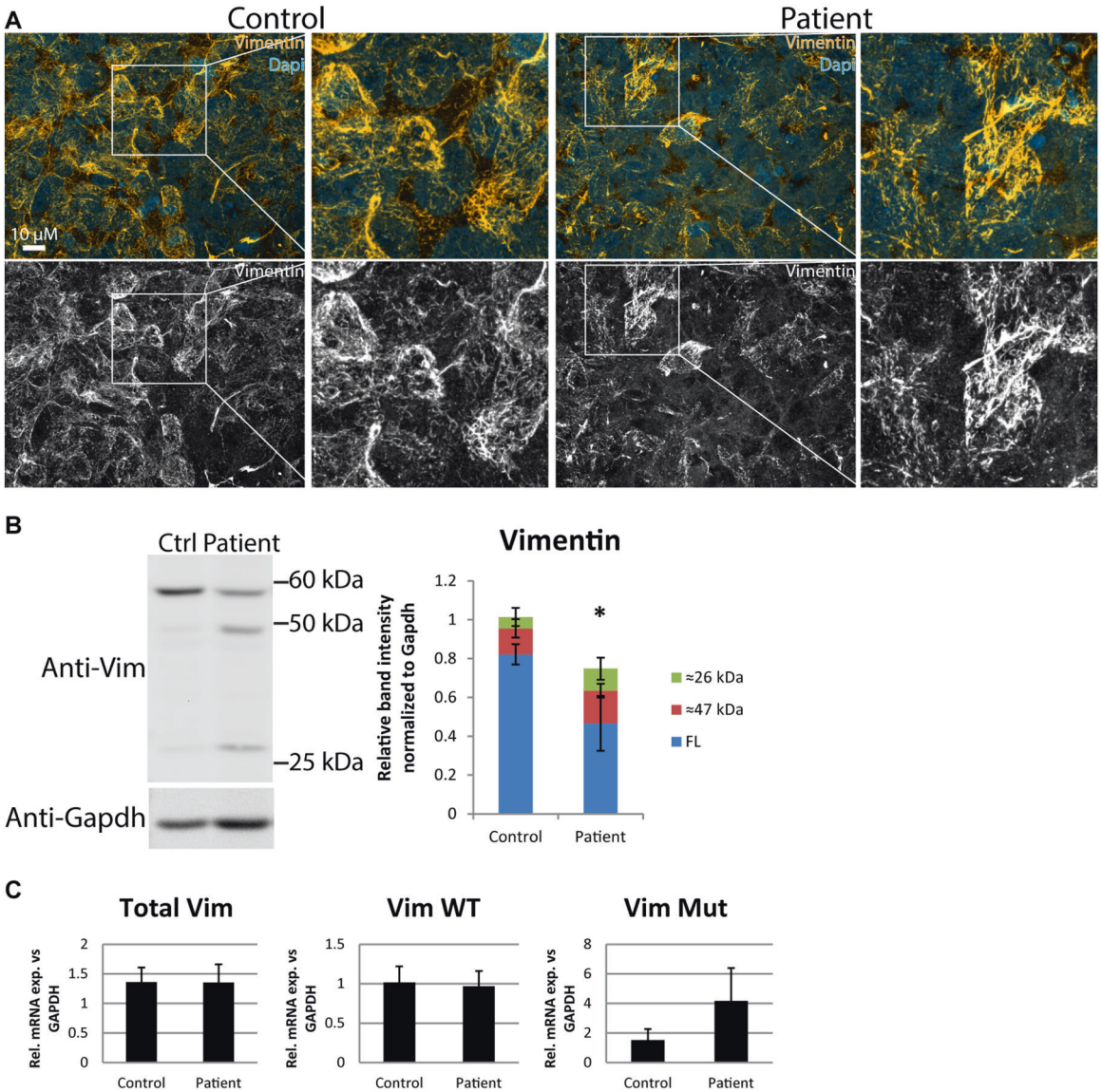

Fig. 3 Vimentin is degraded in the patient's iPS cells. a Immunofluorescence analysis of vimentin in cultured iPS cells derived from a healthy donor (control) and the patient stained for vimentin and nuclei. Note the decreased number of vimentin-positive cells in the patient's cells (see also Supplementary Fig. S1B). **b** Western blot analysis of vimentin and Gapdh in iPS cells showing a reduced vimentin protein amount and an apparent increased processing of vimentin$^{p.(Leu387Pro)}$. **c** Quantitative RT-PCR analysis showing the expression of total vimentin, vimentin$^{p.(Leu387Pro)}$ (wt), and vimentin$^{p.(Leu387Pro)}$ (Mut) in iPS cells.

these vimentin species (Supplementary Fig. S3C). Upon inhibition of total protein biosynthesis by cycloheximide in 3T3-L1/Vim-HA and 3T3-L1/Vim$^{p.(Leu387Pro)}$ -HA cells, the mutant decreased to lower levels than the wt protein, confirming the higher turnover of vimentin$^{p.(Leu387Pro)}$-HA (Fig. 5c).

Overexpression of mutant *vimentin* RNA in zebrafish larvae leads to craniofacial, axonal guidance, and lipid distribution defects

To date, missense variants in IF genes have been described to cause postnatal, tissue-specific diseases [2]. The multi-organ defects, such as malformations of facial bones and of peripheral nerves, identified in our patient were highly suggestive of early-onset defects, possibly with a developmental origin. To challenge this possibility, we chose to utilize the developing zebrafish as an in vivo model. Purified mRNAs encoding human wt *vimentin* or *vimentin*$^{p.(Leu387Pro)}$ were injected into zebrafish one-cell-stage eggs. We first performed an Alcian blue staining of zebrafish larvae at 5 days post fertilization (dpf) to determine whether they bore craniofacial abnormalities upon expression of the human wt or mutated RNA. We observed a significantly increased distance between the ceratohyal and Meckel's cartilages (Fig. 6a) upon overexpression of the wt mRNA, compared

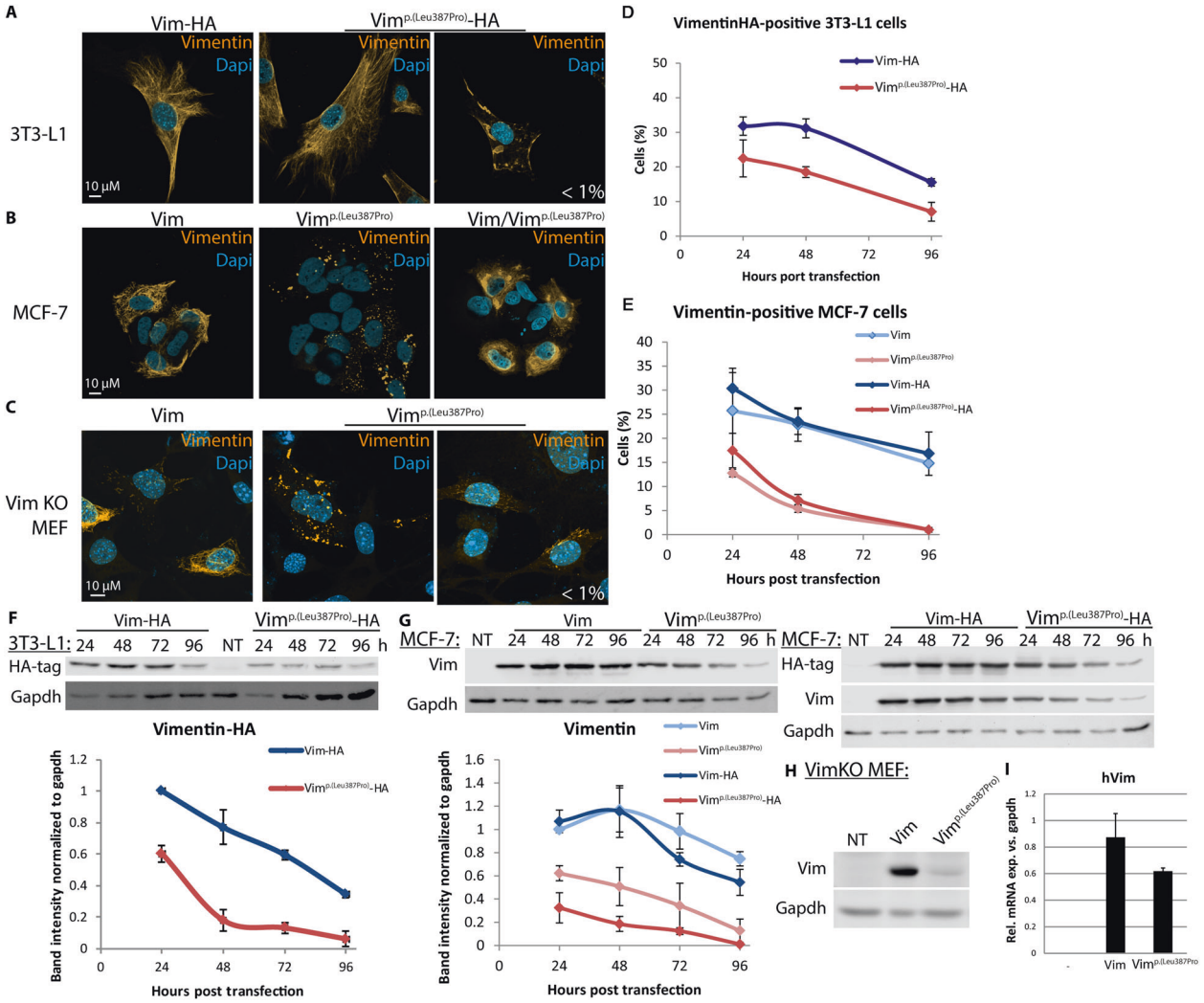

Fig. 4 Vimentin$^{p.(Leu387Pro)}$ forms short-lasting aggregate-like structures in the absence of wt vimentin. a Immunofluorescence analysis of human vimentin in vimentin-positive 3T3-L1-expressing vimentin-HA or vimentin$^{p.(Leu387Pro)}$-HA and stained for HA-tag and nuclei. **b** Immunofluorescence analysis of human vimentin in vimentin-free MCF-7 cells transiently expressing vimentin or vimentin$^{p.(Leu387Pro)}$ or a mixture of both fixed 48 h after transfection and stained for vimentin and nuclei. In absence the wt, vimentin$^{p.(Leu387Pro)}$ is unable to form filaments but forms extensive filaments upon coexpression with wt vim, in addition to a few cells with aggregate-like structures. **c** Immunofluorescence analysis of vimentin in vimentin KO MEF transiently expressing human vimentin or vimentin$^{p.(Leu387Pro)}$ fixed 48 h after transfection and stained for vimentin and nuclei. Note that the mutant protein forms cytoplasmic aggregate-like structures of various sizes. **d** Graph showing more rapid disappearance of mutant compared with wt vimentin-positive transfected 3T3-L1 cells. Corresponding immunofluorescence images are shown in supplement. **e** G Graph showing more rapid disappearance of vimentin$^{p.(Leu387Pro)}$ compared with wt vimentin-positive transfected MCF-7 cells. Corresponding immunofluorescence pictures are shown in supplement. **f** Western blot analysis of HA-tagged vimentin and Gapdh in extracts from 3T3-L1 cells transiently expressing vimentin-HA or vimentin$^{p.(Leu387Pro)}$-HA at several time points after transfection. Relative vimentin band intensities normalized to Gapdh are depicted in the graph. Note the constant lower protein amount of vimentin$^{p.(Leu387Pro)}$ compared with wt vimentin. **g** Western blot analysis of vimentin, HA-tagged vimentin, and Gapdh in extracts from MCF-7 cells transiently expressing vimentin, vimentin$^{p.(Leu387Pro)}$, vimentin-HA, or vimentin$^{p.(Leu387Pro)}$-HA at several time points after transfection. Relative vimentin band intensities normalized to Gapdh are depicted in the graph. Note that although the wt vimentin protein amount starts to decrease 48 h after transfection, the vimentin$^{p.(Leu387Pro)}$ quantities are always lower and start to decrease earlier. **h** Western blot analysis of vimentin and Gapdh in vimentin KO MEF transiently expressing vimentin or vimentin$^{p.(Leu387Pro)}$ showing a drastically reduced mutant protein amount 48 h post transfection. **i** Quantitative RT-PCR analysis showing the expression of human vimentin in cells in the same condition than in **f**.

with age-matched controls (Fig. 6b). Strikingly, we observed an exacerbated effect on the cartilage distance upon overexpression of the *vimentin*$^{p.(Leu387Pro)}$ mRNA compared with the wt mRNA (Fig. 6b).

We next performed a whole-mount immunostaining with an anti-acetylated tubulin antibody on zebrafish larvae at 3 dpf to visualize the well-organized architecture of peripheral axons that extend from the notochord and innervate the

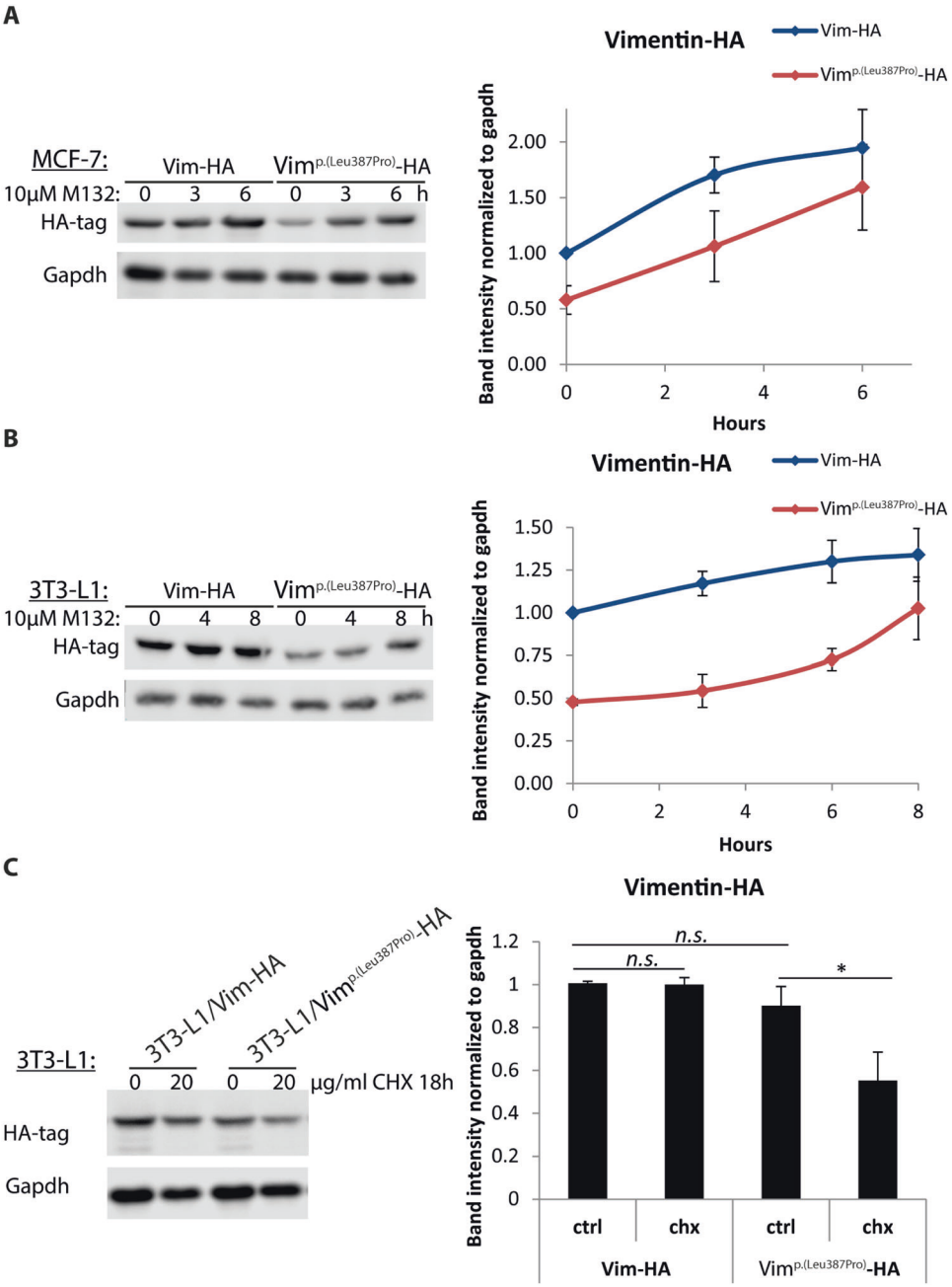

Fig. 5 Vimentin$^{p.(Leu387Pro)}$ proteasomal degradation is accelerated compared with wt vimentin. a Anti-HA and -Gapdh immunoblot analysis of MCF-7 cells transiently expressing vimentin-HA or vimentin$^{p.(Leu387Pro)}$-HA, treated with 10 μM MG-132 (proteasome inhibitor) for the indicated time points. The graphs show the corresponding quantifications, indicating that non-filamentous vimentin$^{p.(Leu387Pro)}$-HA is degraded by the proteasome at a faster rate for the mutant. **b** Anti-HA and -Gapdh immunoblot analysis of and 3T3-L1 cells transiently expressing vimentin-HA or vimentin$^{p.(Leu387Pro)}$-HA, treated with 10 μM MG-132 (proteasome inhibitor) for the indicated time points. The graphs show the corresponding quantifications, indicating that filamentous vimentin$^{p.(Leu387Pro)}$-HA is degraded by the proteasome with a faster rate for the mutant. **c** Anti-HA and -Gapdh immunoblot analysis and corresponding quantification of 3T3-L1/Vim-HA and 3T3-L1/Vim$^{Lp.(Leu387Pro)}$HA cells treated with 20 μg/ml cycloheximide (protein synthesis inhibitor) for 18 h confirming that vimentin$^{p.(Leu387Pro)}$-HA is more rapidly degraded that the wt.

myotomes via a fork-like termination (Fig. 6c). We scored the number of peripheral axons with sprouting and/or pathfinding defects on eight fixed consecutive metameres. Although overexpression of both the wt and the mutant *vimentin*$^{p.(Leu387Pro)}$ RNAs led to a significant number of axonal defects compared with controls, the phenotypic severity is exacerbated in the mutant condition (i.e., no larva injected with the wt mRNA has been scored in the categories "with defects in 5, 6, or 8 axons") (Fig. 6d).

Finally, to measure body fat distribution as a readout for lipodystrophy in zebrafish larvae, we stained lipids of mRNA-injected larvae at 5 dpf with Oil Red O as described [15]. Overexpression of human wt or *vimentin*$^{p.(Leu387Pro)}$ RNA showed a significant lipid accumulation in the gut when compared with controls (Fig. 6e, f). However, no significant difference was observed between wt and mutant at this developmental stage. Taken together, these data suggested that overexpression of wt *vimentin* or *vimentin*$^{p.(Leu387Pro)}$ RNAs disturbed the development of the face, the sprouting, and pathfinding of peripheral axons, and affected fat distribution, with *vimentin*$^{p.(Leu387Pro)}$ displaying exacerbated phenotypes.

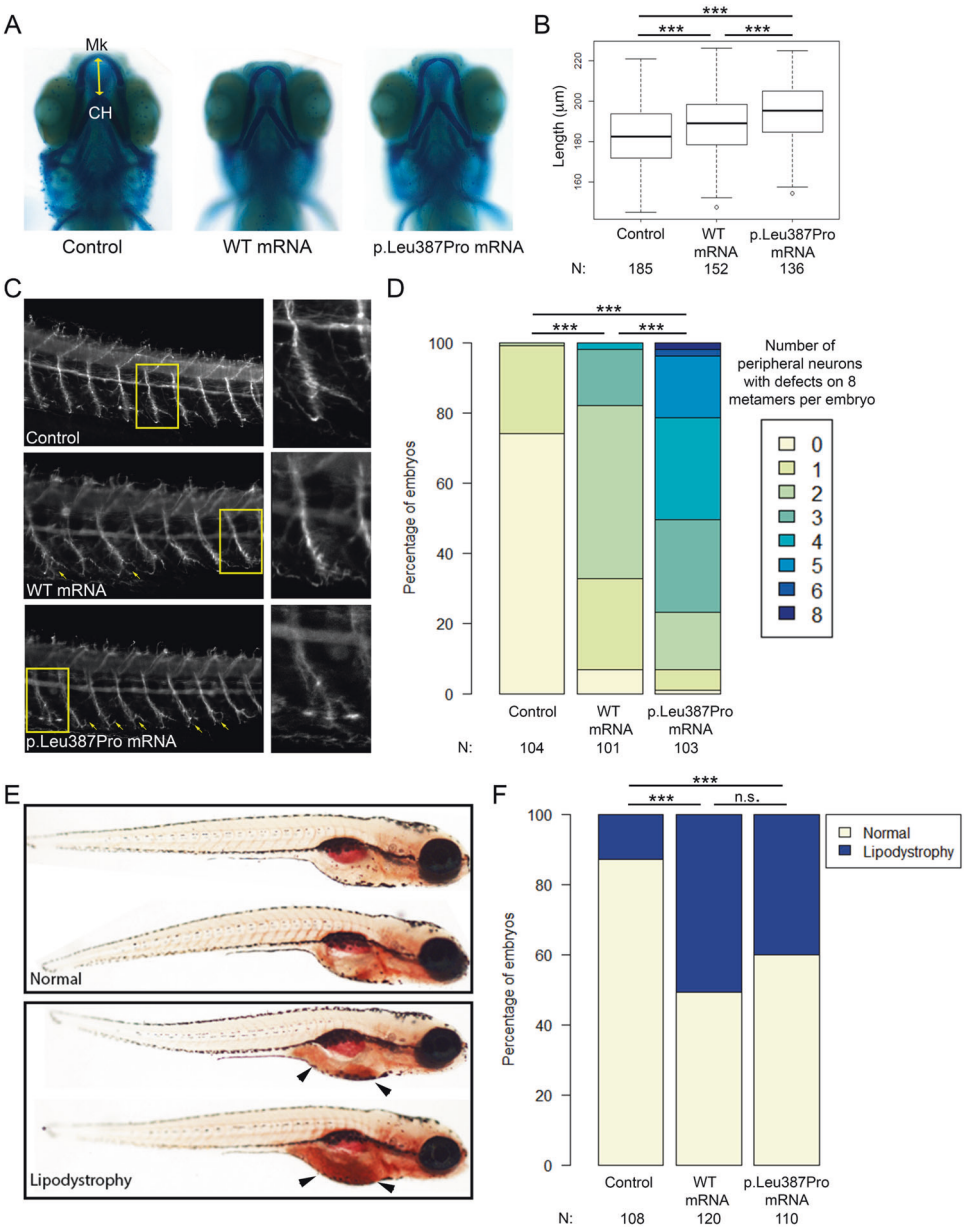

3T3-L1/Vim$^{p.(Leu387Pro)}$-HA adipocytes accumulate less lipid droplets and perilipin than wt vimentin-expressing cells

To gain insight into mechanisms underlying the lipodystrophy, we investigated the impact of vimentin$^{p.(Leu387Pro)}$ during adipogenesis in vitro using 3T3-L1 preadipocytes engineered to express vimentin$^{p.(Leu387Pro)}$-HA and wt vimentin-HA (3T3-L1/Vim-HA cells and 3T3-L1/Vim$^{p.(Leu387Pro)}$-HA cells), in addition to non-transduced controls. Preadipocytes were subjected to an adipogenic differentiation protocol followed by expression analysis of major differentiation genes by reverse-transcriptase quantitative PCR (C/EBPα, β, δ, PPARγ transcription factors, the insulin-regulated glucose transporter GLUT4 and perilipin) and immunoblotting (for C/EBPα, β, and PPARγ). [16] Expression levels of these genes were comparable in all cell lines analyzed (Supplementary Figs. S4A and S6B), indicating that vimentin$^{p.(Leu387Pro)}$ did not affect adipogenic differentiation at the transcriptional level [17]. However, the analysis of lipid droplets revealed a significantly reduced lipid quantity in mutant compared with wt vimentin-expressing and control cells (Fig. 7a, b). Thus, decreased lipid accumulation in cellulo is reminiscent of the patient's lipodystrophy.

Considering that vimentin is known to co-precipitate and colocalize with perilipin-1 (perilipin), which coats the surface of lipid droplets and regulates lipid release from

◀ **Fig. 6 Overexpression of p.(Leu387Pro) *vimentin* RNA in zebrafish larvae leads to craniofacial and axonal guidance defects, and disturbs their lipid storage. a** Representative ventral images of zebrafish larvae injected with sham (control), wt, or *vimentin*$^{p.(Leu387Pro)}$ RNAs at 5 days post fertilization, stained with Alcian blue to visualize craniofacial cartilages. **b** Boxplots of the measured distance between the ceratohyal (CH) and Meckel's (MK) cartilages for each condition tested. Note the increased distance of wt compared with controls (p-value = 0.0009174) and of *vimentin*$^{p.(Leu387Pro)}$ compared with controls (p-value = $6.56.10^{-12}$) or wt (p-value = 0.0003561). *T*-test was conducted between pairs of conditions. **c** Representative lateral images of zebrafish larvae injected with sham (control), wt, or *vimentin*$^{p.(Leu387Pro)}$ RNAs at 3 days post fertilization stained with anti-acetylated tubulin monoclonal antibody to visualize the architecture of peripheral neurons. Peripheral axons can exhibit aberrant number of terminations (see inset of *vimentin*$^{p.(Leu387Pro)}$ mRNA overexpression), fuzzy terminations (see inset of wt *vimentin* mRNA overexpression), or ectopic branching of the axon (not shown). Defective axons are shown by yellow arrows. **d** Percentage of larvae with axon guidance defects according to peripheral neurons staining. The numbers of affected axons were counted for each animal across eight metameres. The bar plots indicate the number of affected axons across eight consecutive metameres for the three tested conditions: larvae batches injected with control, *vimentin*, or *vimentin*$^{p.(Leu387Pro)}$ mRNAs. See the increased number of axonal defects per embryo upon overexpression of *vimentin* or *vimentin*$^{p.(Leu387Pro)}$ compared with age-matched control (p-value = $< 2.2 \times 10^{-16}$), and the increased severity of the phenotype in presence of *vimentin*$^{p.(Leu387Pro)}$. Fifty percent of the larva injected with *vimentin*$^{p.(Leu387Pro)}$ mRNA showed defects in 4 to 8 axons, whereas only 2% of the larva injected with wt mRNA showed defects in 4 axons and no larva injected with the wt mRNA has been scored with defects in 5, 6, or 8 axons. Fisher's exact test was performed between pairs of conditions. **e** Representative lateral images of Oil Red O-stained zebrafish larvae at 5 days post fertilization to visualize the distribution of the lipids. Larvae were classified between normal (normal distribution of lipids) and larvae with lipodystrophy (lipid accumulation in the gut, see black arrowheads). **f** Qualitative scoring of the lipodystrophy in larvae batches injected with control, *vimentin*, or *vimentin*$^{p.(Leu387Pro)}$ mRNAs. Ten percent of the control larva showed lipid accumulation in the gut, whereas 50.8% and 40% of embryos expressing *vimentin* or *vimentin*$^{p.(Leu387Pro)}$, respectively did (p-value = 6.581.10–10 between wt and aged-matched controls; p-value = 6.646.10–06 between *vimentin*$^{p.(Leu387Pro)}$ and aged-matched controls; p-value = 0.1126 between wt and *vimentin*$^{p.(Leu387Pro)}$). Fisher's exact test was performed between pairs of conditions. ***p-value < 0.001. CH ceratohyal cartilage, Mk Meckel's cartilage, N number of embryos per condition.

lipid droplets [18–20], we performed double immunostaining for both perilipin, vimentin, and HA-tagged vimentin, respectively, in the corresponding cells. Consistent with the reduced lipid amount, the number of cells forming large perilipin-positive lipid droplets was reduced by ≈30 % in 3T3-L1/Vim$^{p.(Leu387Pro)}$-HA cells, suggesting that vimentin$^{p.(Leu387Pro)}$ affects late stages of lipid droplet formation or homeostasis (Fig. 7c and Supplementary Fig. S5A, B). Notably, the amount of perilipin was reduced by ≈25 % in 3T3-L1/Vim$^{p.(Leu387Pro)}$-HA compared with that in 3T3-L1/Vim-HA cells (Fig. 7d). The persistent and close association of perilipin-positive lipid droplets with vimentin-HA or vimentin$^{p.(Leu387Pro)}$-HA indicated that vimentin$^{p.(Leu387Pro)}$ mutant did not fully compromise lipid accumulation in the model used, possibly because of the low abundance of vimentin$^{p.(Leu387Pro)}$ (Supplementary Fig. S3C). Taken together, these data suggest that dominant vimentin$^{p.(Leu387Pro)}$ compromises lipid accumulation in parts through destabilization of perilipin.

Discussion

We report here a novel missense variant in *VIM* responsible for a syndrome associating developmental and aging-related features. The vimentin$^{p.(Leu387Pro)}$ mutant impaired craniofacial development, peripheral axon branching, and fat distribution in zebrafish. We also demonstrate that the vimentin$^{p.(Leu387Pro)}$ mutant reduced lipid droplet size and numbers, and negatively regulated the abundance of perilipin during in vitro adipogenesis. Finally, we present evidence for enhanced proteolytic processing and turnover of vimentin$^{p.(Leu387Pro)}$ in patient-derived iPS and in two types of transfected cells.

Unlike most other disease-associated variants in cytoplasmic IF genes reported so far [2, 21], vimentin$^{p.(Leu387Pro)}$ likely affects development. In fact, variants found in *KRT8*, *KRT18*, or *KRT19*, which are expressed before vimentin [22, 23], only predispose to a mild phenotype with adult onset [2, 21]. Moreover, variants in epidermal keratins and desmin, which are responsible for the integrity of strain-exposed cells and tissues [24, 25], manifest perinatally or later, upon the onset of mechanical load.

The Leucine residue at position 387 in vimentin is located in an "e" position along the α-helical wheel of the coil2 subdomain, which is important for early steps of vimentin oligomerization [3]. This amino acid is highly conserved among IF proteins and its substitution in *KRT17* and desmin causes steatocystoma multiplex with oligodontia (MIM: 184500) and myofibrillar myopathy (MIM: 601419), respectively [12, 26] (Fig. 2a). Although consequences for protein stability have not been reported for corresponding *KRT17* and desmin variants, we found a lower abundance of the vimentin$^{p.(Leu387Pro)}$ variant likely due to augmented proteolytic processing and proteasomal turnover (Figs. 4 and 5, and Supplementary Figs. S1, S2). The latter could be caused by an improper folding of vimentin$^{p.(Leu387Pro)}$ protein, as it formed aggregate-like structures in IF-free transfected cells (Figs. 4a, c and Supplementary Fig. S2A).

One of the key clinical features of the patient carrying the vimentin$^{p.(Leu387Pro)}$ variant is a progressive peripheral neuropathy, in line with its early and widespread expression in development [27]. We hypothesize that the early developmental expression of vimentin$^{p.(Leu387Pro)}$ in nearly all neuronal precursors in vivo, before its replacement by neurofilaments shortly after the immature neurons become

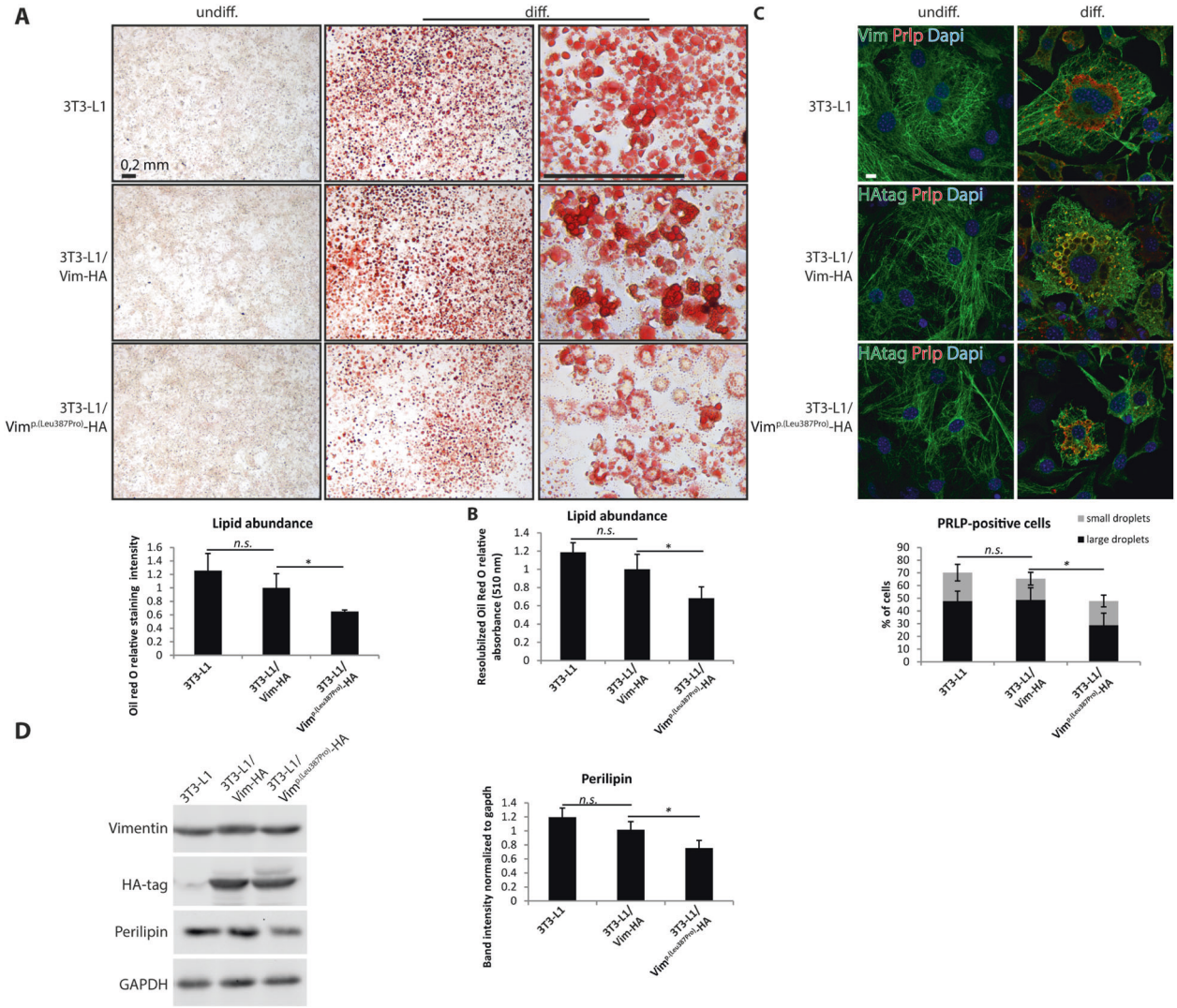

Fig. 7 3T3-L1/Vim$^{p.(Leu387Pro)}$-HA adipocytes accumulate less lipid droplets and perilipin than wt vimentin-expressing cells. a Light microscopy images of 3T3-L1, 3T3-L1/Vim-HA, and 3T3-L1/Vim$^{p.(Leu387Pro)}$-HA preadipocytes and adipocytes 6 days following differentiation, stained for lipids with Oil Red O dye (scale bar: 200 µm). Quantification of images shows that 3T3-L1/Vim$^{p.(Leu387Pro)}$-HA adipocytes store less lipids than 3T3-L1 and 3T3-L1/Vim-HA cells. **b** Relative absorbance (510 nm) measurements of re-solubilized Oil Red O from stained 3T3-L1, 3T3-L1/Vim-HA, and 3T3-L1/Vim$^{p.(Leu387Pro)}$-HA adipocytes, confirming quantifications of cell staining. **c** Confocal immunofluorescence microscopy images of 3T3-L1, 3T3-L1/Vim-HA, and 3T3-L1/Vim$^{p.(Leu387Pro)}$-HA preadipocyte and 6-day adipocytes stained for vimentin or HA-tag (green), perilipin (red), and nuclei (blue) (scale bar: 10 µm). Note the partial reorganization of vimentin, vimentin-HA, and vimentin$^{p.(Leu387Pro)}$-HA around perilipin-positive lipid droplets together with filamentous patterns in differentiated cells. The graph shows the percentage of perilipin-positive cells and indicates a lower amount of cells with large perilipin-positive droplets in 3T3-L1/Vim$^{p.(Leu387pro)}$-HA adipocytes. **d** Immunoblot of vimentin, HA-tag, perilipin, and Gapdh in 3T3-L1, 3T3-L1/Vim-HA, and 3T3-L1/Vim$^{p.(Leu387Pro)}$-HA cells after 6 days of adipogenic differentiation, revealing a decreased amount of perilipin in 3T3-L1/Vim$^{p.(Leu387Pro)}$-HA adipocytes.

post-mitotic, sets the trigger for multiple pathological alterations. Vimentin is also known to support astrocyte migration and the initiation of neurite outgrowth [28, 29]. In our study, we indeed showed that overexpression of human vimentin$^{p.(Leu387Pro)}$ mRNA in zebrafish larvae leads to an altered sprouting and pathfinding of the peripheral axons (Fig. 6c, d). This is in line with recent studies of vimentin KO mice showing a cerebellar defect, impaired motor coordination, hypermyelination, and impaired microglia [27, 30–32]. Moreover, deletion of vimentin in glial fibrillary acidic protein KO mice aggravated a range of glial and neuronal phenotypes [2]. The clinical presentation of the patient also suggested a role of human vimentin during adipogenesis. In line with this, we found that vimentin$^{p.(Leu387Pro)}$ reduced the abundance of perilipin and of large lipid droplets in the well-established 3T3-L1 model (Fig. 7 and Supplementary Figs. S4, S5), without affecting the transcription of key genes governing adipogenesis. It suggests that the decrease in full-length vimentin, which possibly interacts with perilipin through Arg residues located in the N-terminal vimentin head

domain [18], destabilizes perilipin. In support, expression of a dominant-negative acting vimentin mutant in 3T3-L1 pre-adipocytes caused disruption of lipid droplets and increased turnover of triglycerides [33], consistent with the importance of the cage-like vimentin scaffolds engulfing lipid droplets during adipogenesis [18, 19]. Our in vitro data were further confirmed by direct observation of lipid distribution defects in zebrafish (Fig. 6e, f), which is reminiscent of the fat accumulation defects observed in vimentin KO mice [8]. The increase in lipodystrophy upon injection of wt vimentin mRNA is compatible with the notion that transgenic over-expression of wt vimentin caused pathological anomalies in mice [34].

Premature aging remains incompletely understood at the molecular level. A subset of *LMNA* variants cause Hutchison-Gilford Progeria Syndrome (HGPS). The patient described here shares several features with HGPS, such as alopecia, oligodontia, and lipodystrophy, albeit in a milder form. In addition, early onset of neuropathy, deafness, stroke, and glaucoma also clinically evoked a progeroid syndrome.

Remarkably, vimentin knockin mice in which all Ser residues phosphorylated during mitosis were mutated to Ala (vimentin^{SA}) also developed a phenotype compatible with an aging phenotype partially overlapping with our patient's symptoms [9–11]. The vimentin^{SA} mice showed increased neural progenitor differentiation, subcutaneous fat loss, delayed skin wound-healing, elevated expression of senescence markers, aneuploidy, and chromosomal instability. Ultimately, defects in lens epithelial cells resulted in a cataract, reminiscent of the one described earlier in mice transgenic for vimentin p.(Arg113Cys) [7]. Of note, vimentin^{SA} mice of old age suffered from loss of subcutaneous fat. Unlike in vimentin^{SA} and vimentin p.(Arg113Cys) transgenic mice and the patients carrying c.451 G > A p.(Glu151Lys), c.623 A > G p.(Gln208Arg), or c.15delC p.(Val6Cysfs*26) variants, our patient did not develop a cataract. It has been shown that vimentin^{SA} and vimentin$^{p.(Glu115Lys)}$ proteins form cytoplasmic aggregates even in the presence of wt vimentin, while our vimentin staining showed a filament pattern of the variant in the presence of the wt vimentin (Figs. 3a, 4a, and Supplementary Figs. S1, S2B). This difference of protein behavior or the different nature of the variant could explain the absence of a cataract in the patient. Whether the patient might develop a cataract later in life cannot be excluded at present.

Collectively, the data strongly support the view that the complex pathology that results from expression of vimentin$^{p.(Leu387Pro)}$ is much more severe than that of vimentin loss-of-function phenotypes, even if they occur together with another type III IF protein. Apart from a disturbed lipid metabolism, vimentin KO mice and cells do not share obvious phenotypes with any of the reported vimentin mutant mouse models, human diseases, or the vimentin$^{p.(Leu387Pro)}$ variant. We therefore favor the hypothesis that the p.(Leu387Pro) variant causes primarily dominant effects.

Therefore, our data suggest that VIM$^{p.(Leu387Pro)}$ probably acts as a dominant-negative or gain-of-function variant that affects the development and/or homeostasis of a wide range of tissues and organs. We showed that this variant enhances vimentin turnover, which possibly triggers deterioration of multiple organs. The complex pathology resulting from a single vimentin variant likely results from its widespread expression and its heteromeric association with type III and type IV IF proteins, features that set it apart from tissue-restricted IF proteins [2]. Moreover, we presently cannot exclude that some of the other rare variants detected in the patient could contribute to the vimentin$^{p.(Leu387Pro)}$ syndrome described here. However, the occurrence of multisystem disorders following single gene variants is not unique but a hallmark of laminopathies and additional disorders, such as RASopathies [35, 36]. Given the widespread expression of vimentin, we hypothesize that other vimentin variants may trigger similar and additional syndromes, affecting particularly mesoderm-derived tissues. We anticipate that the identification of other vimentin variants by exome or genome analyses will extend the phenotypic spectrum associated with vimentin defects.

Acknowledgements We thank Dr Hans Heid and Professor Harald Herrmann (German Cancer Research Center, Heidelberg, Germany) for providing anti-perilipin antibody and human vimentin cDNA, and Strelkov SV (KU Leuven, Leuven, Belgium) for crosschecking the mutant structure model. We are grateful to the staff of the zebrafish (in particular Sandrine Geschier) and imaging facilities of the Institut de Génétique et de Biologie Moléculaire et Cellulaire. TMM dedicates this work to Prof. Werner W. Franke on the occasion of his 80th birthday.

Funding This work was partially supported by the DFG (Deutsche Forschungsgemeinschaft) (MA1316–15, MA1316–17, MA1316–19, MA1316–21, INST 268/230–1) to TMM and J-EB (MA 1316/15–2), the French Programme Investissements d'Avenir (ANR-10-IDEX-0002–02, ANR-10-LABX-0030-INRT) to CG, and ROTARY Club des Sables d'Olonne to BI. GH is supported by a PhD fellowship (ANR-10-LABX-0030-INRT). DK was supported by the European Research Council under the European Union's Seventh Framework Programme (FP/2007–2013)/ERC-StG2013 337713 DarkSide starting grant.

Author contributions BC, J-EB, CG, TMM, and BI co-designed the study and wrote the manuscript. BC designed and performed exome analysis. J-EB designed and performed the experiments involving mammalian cells and sequence alignments. CG and GH designed and performed the zebrafish experiments. SP, DK, XL, TB, and SK performed molecular biology experiments. PB and BI performed clinical evaluation of the patient. LD, AC, and KS performed patient's cells reprogramming.

Compliance with ethical standards

Conflict of interest The authors declare that they have no conflict of interest.

References

1. Gruenbaum Y, Foisner R. Lamins: nuclear intermediate filament proteins with fundamental functions in nuclear mechanics and genome regulation. Annu Rev Biochem. 2015;84:131–64.
2. Bouameur JE, Magin TM. Lessons from animal models of cytoplasmic intermediate filament proteins. Subcell Biochem. 2017;82:171–230.
3. Chernyatina AA, Guzenko D, Strelkov SV. Intermediate filament structure: the bottom-up approach. Curr Opin Cell Biol. 2015; 32:65–72.
4. Cheng F, Eriksson JE. Intermediate filaments and the regulation of cell motility during regeneration and wound healing. Cold Spring Harb Perspect Biol. 2017;9:pii: a022046.
5. Ma AS, Grigg JR, Ho G, Prokudin I, Farnsworth E, Holman K, et al. Sporadic and familial congenital cataracts: mutational spectrum and new diagnoses using next-generation sequencing. Hum Mutat. 2016;37:371–84.
6. Muller M, Bhattacharya SS, Moore T, Prescott Q, Wedig T, Herrmann H, et al. Dominant cataract formation in association with a vimentin assembly disrupting mutation. Hum Mol Genet. 2009;18:1052–7.
7. Bornheim R, Muller M, Reuter U, Herrmann H, Bussow H, Magin TM. A dominant vimentin mutant upregulates Hsp70 and the activity of the ubiquitin-proteasome system, and causes posterior cataracts in transgenic mice. J Cell Sci. 2008;121:3737–46.
8. Wilhelmsson U, Stillemark-Billton P, Boren J, Pekny M. Vimentin is required for normal accumulation of body fat. Biol Chem. 2019;400:1157–62.
9. Chen M, Puschmann TB, Marasek P, Inagaki M, Pekna M, Wilhelmsson U, et al. Increased neuronal differentiation of neural progenitor cells derived from phosphovimentin-deficient mice. Mol Neurobiol. 2018;55:5478–89.
10. Tanaka H, Goto H, Inoko A, Makihara H, Enomoto A, Horimoto K, et al. Cytokinetic failure-induced tetraploidy develops into aneuploidy, triggering skin aging in phosphovimentin-deficient mmice. J Biol Chem. 2015;290:12984–98.
11. Matsuyama M, Tanaka H, Inoko A, Goto H, Yonemura S, Kobori K, et al. Defect of mitotic vimentin phosphorylation causes microophthalmia and cataract via aneuploidy and senescence in lens epithelial cells. J Biol Chem. 2013;288:35626–35.
12. Olive M, Armstrong J, Miralles F, Pou A, Fardeau M, Gonzalez L, et al. Phenotypic patterns of desminopathy associated with three novel mutations in the desmin gene. Neuromuscul Disord. 2007;17:443–50.
13. Nelson WJ, Traub P. Proteolysis of vimentin and desmin by the Ca2+-activated proteinase specific for these intermediate filament proteins. Mol Cell Biol. 1983;3:1146–56.
14. Fischer S, Vandekerckhove J, Ampe C, Traub P, Weber K. Protein-chemical identification of the major cleavage sites of the Ca2+ proteinase on murine vimentin, the mesenchymal intermediate filament protein. Biol Chem Hoppe Seyler 1986;367:1147–52.
15. Schlegel A, Stainier DY. Microsomal triglyceride transfer protein is required for yolk lipid utilization and absorption of dietary lipids in zebrafish larvae. Biochemistry 2006;45:15179–87.
16. Sarjeant K, Stephens JM. Adipogenesis. Cold Spring Harb Perspect Biol. 2012;4:a008417.
17. Tong Q, Tsai J, Hotamisligil GS. GATA transcription factors and fat cell formation. Drug N Perspect. 2003;16:585–8.
18. Heid H, Rickelt S, Zimbelmann R, Winter S, Schumacher H, Dorflinger Y, et al. On the formation of lipid droplets in human adipocytes: the organization of the perilipin-vimentin cortex. PLoS ONE 2014;9:e90386.
19. Franke WW, Hergt M, Grund C. Rearrangement of the vimentin cytoskeleton during adipose conversion: formation of an intermediate filament cage around lipid globules. Cell 1987;49:131–41.
20. Brasaemle DL, Subramanian V, Garcia A, Marcinkiewicz A, Rothenberg A. Perilipin A and the control of triacylglycerol metabolism. Mol Cell Biochem. 2009;326:15–21.
21. Omary MB. "IF-pathies": a broad spectrum of intermediate filament-associated diseases. J Clin Invest. 2009;119:1756–62.
22. Jackson BW, Grund C, Winter S, Franke WW, Illmensee K. Formation of cytoskeletal elements during mouse embryogenesis. II. Epithelial differentiation and intermediate-sized filaments in early postimplantation embryos. Differentiation 1981;20:203–16.
23. Franke WW, Grund C, Kuhn C, Jackson BW, Illmensee K. Formation of cytoskeletal elements during mouse embryogenesis. III. Primary mesenchymal cells and the first appearance of vimentin filaments. Differentiation 1982;23:43–59.
24. Goldfarb LG, Dalakas MC. Tragedy in a heartbeat: malfunctioning desmin causes skeletal and cardiac muscle disease. J Clin Invest. 2009;119:1806–13.
25. Homberg M, Magin TM. Beyond expectations: novel insights into epidermal keratin function and regulation. Int Rev Cell Mol Biol. 2014;311:265–306.
26. Gass JK, Wilson NJ, Smith FJ, Lane EB, McLean WH, Rytina E, et al. Steatocystoma multiplex, oligodontia and partial persistent primary dentition associated with a novel keratin 17 mutation. Br J Dermatol. 2009;161:1396–8.
27. Colucci-Guyon E, Portier MM, Dunia I, Paulin D, Pournin S, Babinet C. Mice lacking vimentin develop and reproduce without an obvious phenotype. Cell 1994;79:679–94.
28. Boyne LJ, Fischer I, Shea TB. Role of vimentin in early stages of neuritogenesis in cultured hippocampal neurons. Int J Dev Neurosci. 1996;14:739–48.
29. Yabe JT, Chan WK, Wang FS, Pimenta A, Ortiz DD, Shea TB. Regulation of the transition from vimentin to neurofilaments during neuronal differentiation. Cell Motil Cytoskeleton. 2003;56: 193–205.
30. Jiang SX, Slinn J, Aylsworth A, Hou ST. Vimentin participates in microglia activation and neurotoxicity in cerebral ischemia. J Neurochem. 2012;122:764–74.
31. Triolo D, Dina G, Taveggia C, Vaccari I, Porrello E, Rivellini C, et al. Vimentin regulates peripheral nerve myelination. Development. 2012;139:1359–67.
32. Larsson A, Wilhelmsson U, Pekna M, Pekny M. Increased cell proliferation and neurogenesis in the hippocampal dentate gyrus of old GFAP(−/−)Vim(−/−) mice. Neurochem Res. 2004;29:2069–73.
33. Lieber JG, Evans RM. Disruption of the vimentin intermediate filament system during adipose conversion of 3T3-L1 cells inhibits lipid droplet accumulation. J Cell Sci. 1996;109:3047–58.
34. Capetanaki Y, Smith S, Heath JP. Overexpression of the vimentin gene in transgenic mice inhibits normal lens cell differentiation. J Cell Biol. 1989;109:1653–64.
35. Wang Y, Ostlund C, Choi JC, Swayne TC, Gundersen GG, Worman HJ. Blocking farnesylation of the prelamin A variant in Hutchinson-Gilford progeria syndrome alters the distribution of A-type lamins. Nucleus. 2012;3:452–62.
36. Tajan M, Paccoud R, Branka S, Edouard T, Yart A. The RASopathy family: consequences of germline activation of the RAS/MAPK pathway. Endocr Rev. 2018;39:676–700.

Affiliations

Benjamin Cogné[1,2] · Jamal-Eddine Bouameur[3] · Gaëlle Hayot[4,5,6,7] · Xenia Latypova[1,2] · Sundararaghavan Pattabiraman[8] · Amandine Caillaud[2] · Karim Si-Tayeb[2] · Thomas Besnard[1,2] · Sébastien Küry[1,2] · Caroline Chariau[9] · Anne Gaignerie[9] · Laurent David[9,10] · Philippe Bordure[11] · Daniel Kaganovich[8,12] · Stéphane Bézieau[1,2] · Christelle Golzio[4,5,6,7] · Thomas M. Magin[3] · Bertrand Isidor[1,2]

[1] Centre Hospitalier Universitaire de Nantes, Service de Génétique Médicale, 9 quai Moncousu, 44093 Nantes, France

[2] Université de Nantes, CNRS, INSERM, l'institut du thorax, 44000 Nantes, France

[3] Division of Cell and Developmental Biology, Institute of Biology, University of Leipzig, Philipp-Rosenthal-Strasse 55, 04103 Leipzig, Germany

[4] Institut de Génétique et de Biologie Moléculaire et Cellulaire, Illkirch, France

[5] Centre National de la Recherche Scientifique, UMR7104 Illkirch, France

[6] Institut National de la Santé et de la Recherche Médicale, U1258 Illkirch, France

[7] Université de Strasbourg, Strasbourg, France

[8] Department of Experimental Neurodegeneration, University Medical Center Göttingen, Walweg 33, 37073 Göttingen, Germany

[9] Nantes Université, CHU Nantes, Inserm, CNRS, SFR Santé, FED 4203, Inserm UMS 016, CNRS UMS 3556, F-44000 Nantes, France

[10] Nantes Université, CHU Nantes, Inserm, Centre de Recherche en Transplantation et Immunologie, UMR 1064, ITUN, F-44000 Nantes, France

[11] Centre Hospitalier Universitaire de Nantes, Service Oto-rhino-laryngologie, 9 quai Moncousu, 44093 Nantes, France

[12] 1 Base Pharmaceuticals, 9A Monument Square, #2A, Boston, MA 02129, USA